Investigating the Orientation of Low-Latitude Amplitude Fade Patterns Using a Local Array of GNSS-Based Scintillation Monitors

Isaac G. Wright, Josemaría Gomez Socola, and Fabiano S. Rodrigues

Abstract – Adequate understanding and modeling of ionospheric scintillation patterns are required for proper interpretation of measurements and derivation of plasma parameters. Therefore, we revisited modeling and measurement efforts related to the orientation of low-latitude L-band (∼1–2 GHz) scintillation fade patterns. We deployed a local (<1 km) array of low-cost global navigation satellite system–based scintillation monitors at the Jicamarca Radio Observatory in Peru. The array was used to experimentally determine the orientation of fades by cross-correlating the amplitude scintillation patterns measured by monitors. We also expanded a model of the fading orientation based on the projection of geomagnetic field-aligned irregularities. The results show that the measured orientations strongly agree with model predictions (R = 0.969). The results also help to resolve discrepancies in previous efforts to validate the magnetic field projection model. Finally, the results indicate the potential for extracting information about the height of the scintillation-causing irregularity layer using a locally distributed array of monitors.

1. Introduction

The diffraction patterns associated with low-latitude scintillation, or scintillation fade patterns, can be described as highly anisotropic. For instance, analyses by spaced scintillation monitors deployed at the low-latitude site of Cachoeira Paulista, Brazil (17° magnetic latitude), showed that, for up to 1 km in the magnetic meridional direction, there was no discernible difference in the received intensity fluctuations [1]. The elongation of scintillation fade patterns has been explained by the geomagnetic field alignment of ionospheric irregularities. Irregularities originate at the magnetic equator through a phenomenon known as Equatorial Spread F [2]. Owing to electric fields and upward drifts, these irregularities rise and then "map" along field lines to the equatorial ionization anomaly (EIA) crests, where high-background densities create favorable conditions for the world's strongest scintillations to occur [3].

Manuscript received 5 March 2025. The work at UT Dallas was supported by the NSF Graduate Research Fellowship Program under Grant No. (2136516), by an NSF Award AGS-2432609, and by the Eugene McDermott Foundation.

Isaac G. Wright, Josemaria Gomez Socola, and Fabiano S. Rodrigues are with the William B. Hanson Center for Space Sciences at The University of Texas at Dallas, Richardson, Texas 75080, USA; e-mail: igw180000@utdallas.edu, Josemaria.GomezSocola@utdallas.edu, Fabiano@utdallas.edu.

The orientation in which scintillation fade patterns are elongated is a fundamental property of scintillation and a key consideration in various scintillation analyses, such as the spaced-receiver technique for measuring irregularity drifts [4]. The spaced-receiver technique uses the time delay of signal fading received by two or more receivers to estimate the drifts of the irregularities that cause scintillation. This is advantageous because while monitoring ionospheric dynamics can be done using various instruments, including radar (e.g., [5]), satellite in situ measurements (e.g., [6]), or ionosondes (e.g., [7]), these instruments are relatively expensive and limited in temporal or spatial coverage. In contrast, the spaced receiver technique can be implemented using only two scintillation receivers. Furthermore, the technique is made even more promising by new advancements in low-cost global navigation satellite system (GNSS) hardware [8]. For instance, [9] applied the spaced-receiver technique with low-cost GNSS-based scintillation monitors to measure low-latitude irregularity zonal drifts using signals from geostationary satellites.

Assuming that the irregularities that cause scintillation are aligned with the geomagnetic field, [1] modeled scintillation fade pattern orientations from a projection of the geomagnetic field vector and attempted to validate it with measurements. While the model proved accurate in some regimes, it was not valid for measurements that used signals propagating within 60° of the geomagnetic field vectors (∼2/3 of the total data). Ultimately, "no compelling explanation" was found for the cause of discrepancies. Points within the 60° cone were excluded from the remaining analysis. Although [4] expanded on the technique, experimental validation of their model for scintillation pattern orientations was not conducted. Resolving this discrepancy is crucial for the accurate interpretation of scintillation patterns, and the proper estimation of ionospheric parameters using the spaced receiver technique.

Given these complexities, the importance of fundamental and applied studies of scintillation, and the emergence of low-cost scintillation monitors, we aimed to contribute to studies of the orientations of low-latitude scintillation fade patterns.

2. Methodology

2.1. Experimental Setup

To revisit the studies of the orientation of scintillation patterns, we deployed an array of three scintillation

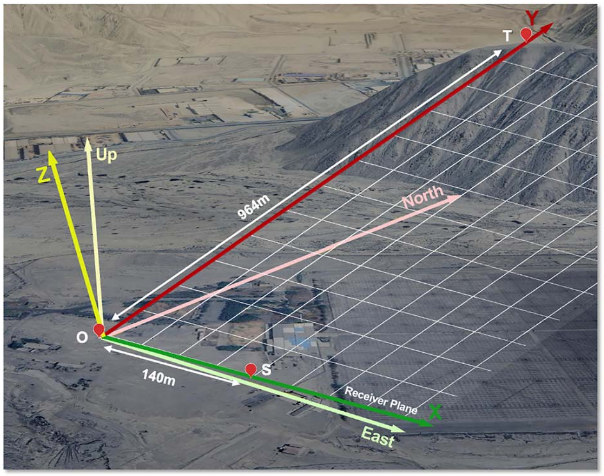

Figure 1. Experiment array at the JRO. Receivers are labeled T, O, and S. Geographic ENU and RCS axes are shown in light and darker colors, respectively. Background image from *Google Earth*.

(ScintPi) monitors at the Jicamarca Radio Observatory (JRO) in Peru (11.97° S, 76.87° W, ∼0° dip latitude). Measurements were made between March 10 and March 19, 2023. ScintPi is a multi-constellation monitor created using Raspberry Pi single-board computers and low-cost, commercial, off-the-shelf GNSS receivers [8]. Carrier-to-noise ratio (C/No) measurements were made at a rate of 20 Hz and with a resolution of 1 dB-Hz from the following GNSS transmissions (∼1.6 GHz): L1 GPS; G1 GLONASS; E1 Galileo; and B1 BeiDou. The monitors were set up for short-term ($<$10 days) autonomous outdoor operation using batteries [10]. The experiment was conducted in March to maximize the likelihood of observing scintillation [2]. Figure 1 shows the configuration of the experiment array. The array consisted of receivers labeled T, O, and S. Receivers O and T were aligned 964 m apart in the magnetic meridian. Receivers O and S formed a baseline 140 m in the magnetic zonal direction. The zonal spacing was a compromise between the Fresnel scale (∼500 m) and preserving high cross-correlation values, consistent with comparable studies using similar baselines [9].

As depicted in the diagram, the receiver plane had an approximate 10° tilt, with receiver T being 177 m higher than receiver O. While the tilt complicates the projection geometry, such a setup is not uncommon. Scintillation receivers are often installed on top of buildings, for instance, with height differences of the same order of inter-receiver distances. This scenario motivated us to generalize our projection model for application to any receiver plane.

Because we will be comparing orientations on a tilted plane, it is useful to define the receiver coordinate system (RCS). The RCS is an orthogonal coordinate frame oriented such that all three receivers lie in the xy plane (receiver plane), with receivers T and O aligned along the y-axis. The unit vectors of RCS are shown in dark colors in Figure 1. For reference, the axes of geographic East-North-Up (ENU) coordinates are shown in light colors. After defining our coordinate system, the transformation from ENU to RCS can be expressed with a generalized rotation matrix, R_{RCS} [11]:

$$R_{RCS} = [\hat{x}_{RX} \quad \hat{y}_{RX} \quad \hat{z}_{RX}] \tag{1}$$

Where $\hat{x}_{RX}$, $\hat{y}_{RX}$, $\hat{z}_{RX}$ are the orthogonal axes vectors of the RCS expressed in ENU. These vectors can be expressed from the ENU receiver baselines, such as:

$$\hat{y}_{RX} = \overrightarrow{\mathrm{OT}} \tag{2}$$

$$\hat{z}_{RX} = \overrightarrow{\mathrm{OS}} \times \overrightarrow{\mathrm{OT}} \tag{3}$$

$$\hat{x}_{RX} = \overrightarrow{\mathrm{OT}} \times \hat{z}_{RX} = \overrightarrow{\mathrm{OT}} \times \left(\overrightarrow{\mathrm{OS}} \times \overrightarrow{\mathrm{OT}}\right) \tag{4}$$

2.2. Measuring Scintillation Fade Pattern Orientation

We determine the orientation of moving scintillation fade patterns using the approach outlined in [1], and summarize as follows. The scintillation fade pattern is described as a plane wave in the receiver plane, having a normal vector $\vec{k}$ and velocity $\vec{v}$. The orientation of the scintillation fade pattern projected onto the receiver plane is defined by the projection angle ϕ, which can be related to $\vec{k}$ as $\vec{k} = \cos\phi, -\sin\phi$. Here, we use the notation that ϕ is measured clockwise from the y-axis. We chose to neglect time-evolution effects of the scintillation pattern, as such corrections are typically minor (∼4% difference [1]), and, more importantly, our analysis depends only on the relative velocity contributions. Assuming a “frozen-in” scintillation pattern, the time lag between the signals received in stations is related to the components of the distance and velocity that are perpendicular to the wavefront, that is, parallel to $\vec{k}$ [1]:

$$\vec{v} \cdot \vec{k} = \frac{\vec{a} \cdot \vec{k}}{\tau_a} = \frac{\vec{b} \cdot \vec{k}}{\tau_b} \tag{5}$$

Where $\vec{a}$ and $\vec{b}$ are the two receiver baseline vectors, and τ_a and τ_b are the respective time lags. We compute the time lag τ between two receivers as the lag, where the cross-correlation of C/No measurements attains its maximum value ρ_{max}. This is a straightforward approach, but as noted in [12], alternative methods, such as spectral decomposition, can be used to examine different drift behaviors at different fluctuation scales. After correlation, (5) is combined with the definition of $\vec{k}$ to solve for the projection angle ϕ.

We identified scintillation events by computing the S_4 index, which can be described as the standard deviation of signal intensity measured over 1 minute normalized by its mean value [13]. To minimize the use

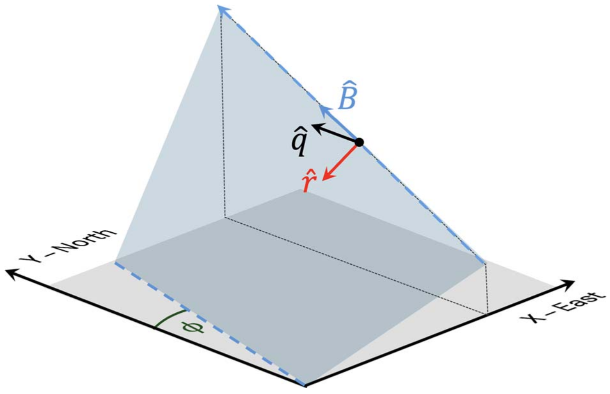

Figure 2. Illustration of projection geometry. The plane formed by $\vec{r}$ and $\overrightarrow{B}$ allows for calculating the projection of $\overrightarrow{B}$ onto the xy plane, whose angle is represented by ϕ. Note that magnetic declination is nearly zero at JRO.

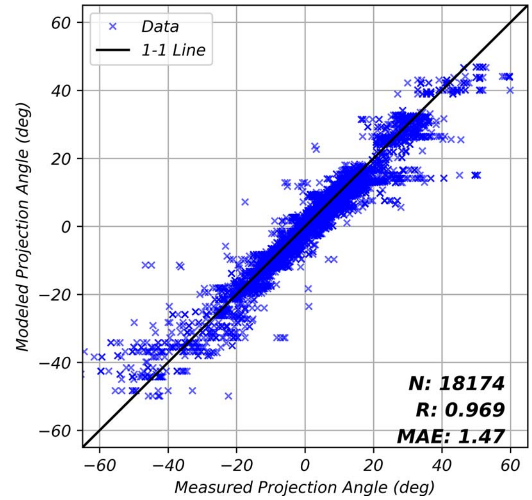

Figure 3. Comparison of projection angles obtained experimentally (measured ϕ) and using the field-aligned model (modeled ϕ).

of measurements affected by multipath, we only considered data for satellite elevation $> 10°$ and $S_4 > 0.2$. We also required $\rho_{max} > 0.7$ because one would not expect C/No fading from multipath to be well-correlated in receivers spaced several hundred meters apart. At the JRO, scintillation severity is typically weak due to its magnetic equatorial position and reduced density deviations compared with the EIA [14]. Nonetheless, a significant number of scintillation events ($S_4 > 0.3$) were observed on four of nine observation nights.

2.3. Modeling Scintillation Fade Pattern Orientation

Owing to the equipotential field line assumption, plasma irregularities are thought to elongate along the geomagnetic field line [15]. Therefore, scintillation patterns are assumed to be oriented along the geomagnetic field lines. Here, we must point out that measurements made by a two-dimensional array of receivers capture the projection of the irregularity distribution onto the array plane. This projection can be modeled by considering the plane spanned by the satellite-receiver ray path vector $\vec{r}$ and the geomagnetic field vector $\overrightarrow{B}$ [6]. The normal vector for this plane is $\vec{q} = \overrightarrow{B} \times \vec{r}$ as illustrated in Figure 2. The line formed by the intersection of the $\vec{q}$ plane with the receiver plane represents the projection of $\overrightarrow{B}$. We track the orientation of this projection using the projection angle ϕ. Here, we use the notation that ϕ is the angle the projected magnetic field vector makes with the RCS y-axis. The projection angle in the receiver plane can be found as:

$$\tan\phi = \frac{-q_y}{q_x} = \frac{-B_x r_z + B_z r_x}{B_y r_z - B_z r_y} \tag{6}$$

Where vectors are in RCS coordinates. $\vec{r}$ is expressed in terms of azimuth (θ) and elevation (φ) angles as:

$$\vec{r} = -\sin(\theta)\cos(\varphi), \cos(\theta)\cos(\varphi), \sin(\varphi) \tag{7}$$

Which can be expressed in RCS as the product $R_{RCS}\vec{r}$.

The International Geomagnetic Reference Field 13 [16] was used to compute $\overrightarrow{B}$ at each Ionospheric Piercing Point (IPP), assuming a thin spherical shell ionosphere at an altitude of 350 km. To transform between ENU at the IPP and ENU at the receiver array, we used Earth Centered Earth Fixed (ECEF) coordinates, which is a Cartesian coordinate system defined independently of the observer. The full transformation M that maps $\overrightarrow{B}$ from the local ENU at the IPP (longitude λ_{IPP} and latitude ξ_{IPP}) to the RCS at the receiver array (longitude λ_{RX} and latitude ξ_{RX}) is expressed as a product of rotation matrices:

$$M = R_{RCS}\ R_{ENU}(\lambda_{RX}, \xi_{RX})\ R_{ECEF}(\lambda_{IPP}, \xi_{IPP}) \tag{8}$$

Where R_{ECEF} is the rotation matrix from ENU to ECEF, and R_{ENU} is its inverse from ECEF to ENU [17].

3. Results and Discussions

3.1 Model Validation

Figure 3 compares the projection angles measured by the array of receivers at the JRO and projection angles predicted by the model described in Section 2.3 (6). The comparison uses a total of $N = 18,174$ ϕ values obtained during the entire observation campaign. We found that scintillation measurements occurred predominantly within two, somewhat specific regions in the sky, north or south of the JRO, and at low elevation angles ($<30°$). These regions correspond to locations of elevated background ionospheric densities associated with the northern and southern EIA peaks. The experiment at the JRO, nevertheless, provided observations of projection angles over a wide range of values, spanning

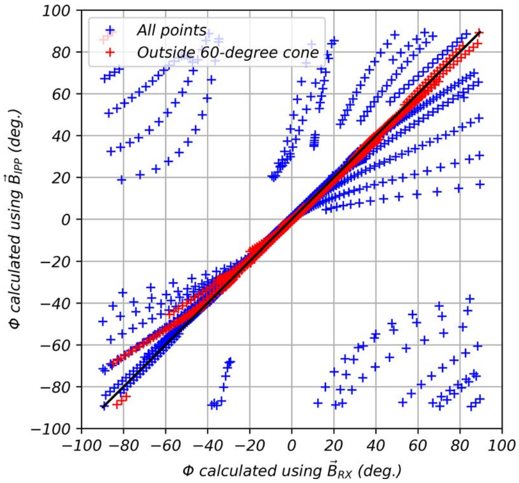

Figure 4. Comparison of ϕ computed using $\overrightarrow{B}_{IPP}$ and $\overrightarrow{B}_{RX}$ with respect to a receiver array located at the low-latitude site of Cachoeira Paulista, Brazil, and GPS ephemerides in 2001.

from $-60°$ to $+60°$. More importantly, the campaign results show an excellent agreement between the model and observations. For instance, the Pearson correlation coefficient (R) for the model and the measurements shown in Figure 3 is 0.969, indicating a strong correlation. Additionally, the mean absolute error (MAE) of the fit was 1.47°.

3.2 Relevance to Previous Studies

Our results led us to hypothesize that the choice of $\overrightarrow{B}$ during the calculations carried out by [1] caused the discrepancies between modeled and observed projection angles in their study. As noted in [4], the study [1] used a different approach to calculate the projection angles, which incorporated a trigonometric model and assumed $\overrightarrow{B}$ to be that at the receiver array location ($\overrightarrow{B}_{RX}$). We point out that $\overrightarrow{B}$ used in the calculation should be computed at each IPP location to best represent the projection geometry. Furthermore, because ϕ is related to $\vec{r} \times \overrightarrow{B}$, the difference in ϕ due to this choice of $\overrightarrow{B}$ will be larger when the angle between $\vec{r}$ and $\overrightarrow{B}$ is smaller. This can be seen by considering the small vector residual $\delta\overrightarrow{B} \equiv \overrightarrow{B}_{RX} - \overrightarrow{B}_{IPP}$ and the product $\vec{r} \times \overrightarrow{B}_{RX} = \vec{r} \times (\overrightarrow{B}_{IPP} + \delta\overrightarrow{B})$. When $|\vec{r} \times \overrightarrow{B}_{IPP}| \ll |\vec{r} \times \delta\overrightarrow{B}|$, $\tan\phi$ approaches $\frac{-(\vec{r} \times \delta\overrightarrow{B})_y}{(\vec{r} \times \delta\overrightarrow{B})_x}$. This would explain the larger discrepancies in the data in the 60° cone. We also highlight that, for observations at JRO, located near the magnetic equator, using a single value ($\overrightarrow{B}_{RX}$) would not have been acceptable. The magnetic dip of approximately 0° would yield nearly constant values of ϕ.

To test our hypothesis, we evaluated the impact of using a single value for $\overrightarrow{B}$ ($\overrightarrow{B}_{RX}$) instead of the $\overrightarrow{B}$ value at the IPP ($\overrightarrow{B}_{IPP}$). The evaluation considered a receiver array located at the low-latitude site of Cachoeira Paulista (22° S, 45° W) and GPS ephemerides from 2001 [18], the same year and location as the experiment conducted by [1]. For this evaluation, we computed ϕ using (6) over GPS satellite tracks between 19:00 and 01:00 LT, with an elevation mask of 10°.

Figure 4 presents the results of our evaluation. It illustrates how the projection angles estimated using $\overrightarrow{B}_{IPP}$ and $\overrightarrow{B}_{RX}$ compare. Most importantly, the distribution demonstrates that the choice of $\overrightarrow{B}$ can lead to large discrepancies between the model and measurements. The results are similar to the discrepancies observed by [1] in calculating ϕ using $\overrightarrow{B}_{RX}$. For instance, we point out the similarity in the increased discrepancy for large projection angles [1]. Also, the simulation confirms that, like [1], the discrepancies are minimized when signals propagating within a 60° cone with respect to $\overrightarrow{B}$ are excluded.

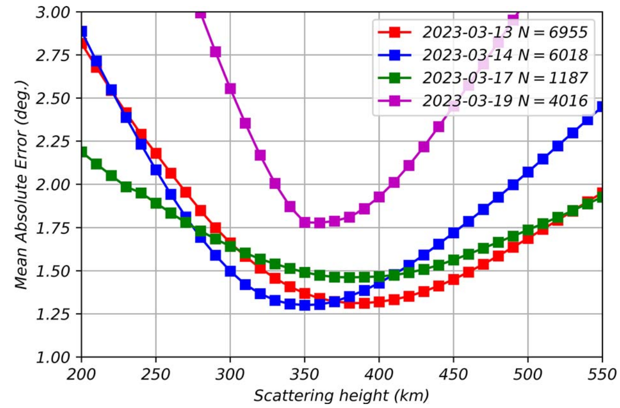

Figure 5. Mean scattering height of the IPP versus MAE of the projection angle model for four days of the observation campaign.

3.3 Estimating Mean Scattering Heights

As described in previous sections, modeling scintillation fade pattern orientations relies on IPPs and assumptions about the mean height of the ionospheric irregularity layer contributing to scattering and diffraction. A layer height of 350 km reflects the nominal height of the ionospheric F-region peak and is commonly used in IPP calculations [19]. Here, we examine the impact of irregularity height in the estimation of projection angles and present an approach for estimating mean scattering heights from the observed projected angles. Figure 5 illustrates our analyses and preliminary results. It shows MAE values computed for observed and model projection angles (ϕ) as a function of mean irregularity height. The results are for four different nights during the campaign.

The results in Figure 5 show that well-defined minima in MAE can be identified each day. Minimum MAE values were found at 390 km, 350 km, 380 km, and 360 km for the datasets corresponding to March 13, 14, 17, and 19, respectively. These results can be interpreted as the mean scattering height of irregularities during the times when scintillation was observed, between approximately 19:00 and 01:00 LT. We interpret the width of the curvatures as representative of the variance of the scattering height estimate throughout the measurements.

Overall, these results are consistent with our initial estimate of 350 km and with the common assumption that ionospheric irregularities contributing the most to scintillation are located near F-region peak heights [2]. These findings also illustrate the potential of local array observations to provide information about mean irregularity heights. This information can be used, for instance, as input in models of radio propagation that require specification of irregularity height.

4. Conclusions

We revisited studies of the orientation of low-latitude scintillation patterns. As part of the effort, we improved a model of the scintillation pattern (projected magnetic field model). Then, we validated our model by experimenting at the Jicamarca Radio Observatory using an array of low-cost GNSS-based scintillation monitors. Key findings are summarized as follows.

We found that the improved model accurately described the observed orientations ($R = 0.969$). These results also indicate that, even at the magnetic equator where the projection geometry is limited, orientations can deviate by as much as 60° from the local magnetic meridian, emphasizing the need to account for this geometry in scintillation studies. Our work also helped to resolve a discrepancy in modeled and observed scintillation pattern orientations [1]. We built upon previous work [4] by experimentally validating their model for the orientation of scintillation patterns and extending it to account for projections onto a non-level planes. We also demonstrate that the discrepancy observed by [1] is resolved by considering the geomagnetic field vector at the IPP location. Finally, we proposed and showed preliminary results of a method to estimate the mean height of ionospheric irregularities responsible for scintillation.

5. Acknowledgments

The authors thank the staff of the Jicamarca Radio Observatory (JRO) for technical support. JRO is a facility of the Instituto Geofisico del Peru operated with support from the NSF AGS-2213849 through Cornell University.

6. References

1. P. M. Kintner, B. M. Ledvina, E. de Paula, and I. J. Kantor, “Size, Shape, Orientation, Speed, and Duration of GPS Equatorial Anomaly Scintillations, *Radio Science*, **39**, 2, April 2004.
2. M. C. Kelley, “Equatorial Plasma Instabilities,” In: M. C. Kelley (ed.), *The Earth’s Ionosphere*, Amsterdam, Elsevier, 1989, pp. 113-185.
3. P. M. Kintner, B. M. Ledvina, and E. R. de Paula, “GPS and Ionospheric Scintillations,” *Space Weather*, **5**, 9, September 2007, p. S09003.
4. B. M. Ledvina, P. M. Kintner, and E. R. de Paula, “Understanding Spaced-Receiver Zonal Velocity Estimation,” *Journal of Geophysical Research*, **109**, A10, 2004.
5. R. F. Woodman, “Vertical Drift Velocities and East-West Electric Fields at the Magnetic Equator,” *Journal of Geophysical Research,* **75**, 31, November 1970, pp. 6249-6259.
6. R. A. Heelis, R. A. Stoneback, M. D. Depew, W. A. Morgan, M. W. Mankey, et al., “Ion Velocity Measurements for the Ionospheric Connections Explorer,” *Space Science Reviews*. **212**, 1-2, July 2017, pp. 615-629.
7. B. W. Reinisch, J. L. Scali, and D. L. Haines, Ionospheric Drift Measurments with Ionosondes,” *Annali di Geofisica,* **41**, 5-6, November 1998, pp. 695-702.
8. J. Gomez Socola and F. S. Rodrigues, “ScintPi 2.0 and 3.0: Low-Cost GNSS-Based Monitors of Ionospheric Scintillation and Total Electron Content,” *Earth Planets and Space*, **74**, 185, December 2022.
9. J. Gomez Socola, F. Rodrigues, I. Wrigth, I. Paulino, and R. Buriti, “ScintPi Measurements of Low-Latitude Ionospheric Irregularity Drifts Using the Spaced-Receiver Technique and SBAS Signals,” *Atmosphere Measurment Techniques*, **18**, February 2025, pp. 909-919.
10. I. G. Wright, I. Solanki, A. Desai, J. Gomez Socola, and F. S. Rodrigues, “Student-Led Design, Development And Tests Of An Autonomous, Low-Cost Platform For Distributed Space Weather Observations,” *Journal of Space Weather and Space Climate*, **13**, 12, April 2023.
11. G. Strang, *Linear Algebra and Its Applications*, Boston, Cengage Learning, 2006.
12. D. Jones and A. D. Maude, “Analysis of Artificial Fading Records,” *Journal of Atmospheric and Terrestrial Physics*, **30**, 5, 1968, pp. 975-977.
13. Y. K. Chie and C.H. Liu, “Radio Wave Scintillations in the Ionosphere,” *Proceedings of the IEEE*, **70**, 4, 1982, pp. 324-360.
14. E. de Paula, F. S. Rodrigues, and K. N. Iyer, “Equatorial Anomaly Effects on GPS Scintillations in Brazil,” *Advances in Space Research*, **31**, 3, February 2003, pp. 749-754.
15. D. T. Farley Jr., “A Theory of Electrostatic Fields in a Horizontally Stratified Ionosphere Subject to a Vertical Magnetic Field,” *Journal of Geophysical Research*, **64**, 9, September 1959, pp. 1225-1233.
16. P. Alken et al., “International Geomagnetic Reference Field: The Thirteenth Generation,” *Earth, Planets and Space*, **73**, 1, February 2021.
17. J. Zhu, “Conversion of Earth-centered Earth-Fixed Coordinates to Geodetic Coordinates,” *IEEE Transactions on Aerospace and Electronic Systems*, **30**, 3, 1994, pp. 957-961.
18. International GNSS Service (IGS), “GNSS Final Combined Orbit Solution Product,” NASA Crustal Dynamics Data Information System, 1992, doi:10.5067/GNSS/GNSS_IGSORB_001.
19. P. V. S. Rama Rao, K. Niranjan, D. S. V. V. D. Prasad, S. Gopi Krishna, and G. Uma, “On the Validity of the Ionospheric Pierce Point (IPP) Altitude of 350 km in the Indian Equatorial and Low-Latitude Sector,” *Annales Geophysicae*, **24**, 2006, pp. 2159-2168.